Crystals 2022

Type of the Paper (Proceedings)

Effects of co-addition of copper, sodium and ethylammonium to $CH_3NH_3PbI_3$ perovskite compound

Riku Okumura [1], Takeo Oku [1,*], Atsushi Suzuki [1], Masanobu Okita [2], Sakiko Fukunishi [2], Tomoharu Tachikawa [2], Tomoya Hasegawa [2]

[1] Department of Materials Science, The University of Shiga Prefecture, 2500 Hassaka, Hikone, Shiga 522-8533, Japan; oe21rokumura@ec.usp.ac.jp (R.O.); suzuki@mat.usp.ac.jp (A.S.)
[2] Osaka Gas Chemicals Co., Ltd., 5-11-61 Torishima, Konohana-ku, Osaka 554-0051, Japan; okita@ogc.co.jp (M.O.); fukunishi@ogc.co.jp (S.F.); t-tachikawa@ogc.co.jp (T.T.); hasegawa_tomoya@ogc.co.jp (T.H.)
* Correspondence: oku@mat.usp.ac.jp; Tel.: +81-749-28-8368

Abstract: From the band calculation, the copper d-orbital band formed slightly above the valence band maximum would function as an acceptor level promoting the generation of carriers. In addition, the excitation processes from the p-orbital of iodine and the d-orbital of copper to the s-orbital of sodium could suppress carrier recombination. Total energy calculations showed that, the stability of the crystal structure decreases with the addition of copper and sodium, but increases with the addition of ethylammonium. Therefore, it is expected that the combination of these compounds can compensate for the disadvantage of unstable crystal structure. The calculated results could be obtained by optimizing the composition of the perovskite and the annealing conditions.

Keywords: copper; sodium; ethylammonium; first-principles calculations; perovskite; solar cell

Citation: Lastname, F.; Lastname, F.; Lastname, F. Title. *Chem. Proc.* **2021**, 3, x. https://doi.org/10.3390/xxxxx

Published: date

1. Introduction

There have been many investigations to improve the conversion efficiency and durability of devices by adding compounds to the perovskite precursor solution, and these are still being actively researched. In this study, copper (Cu), sodium (Na) and ethylammonium (EA) were focused on. Cu compounds are mainly used as hole transport materials, such as copper thiocyanate (CuSCN) and copper oxide (CuO or Cu_2O), which are expected to be stable inorganic hole transport materials that can replace organic hole transport materials [1-5]. Many studies have been reported on the addition of alkali metals to perovskite precursor solutions [6-11], but relatively few studies have been reported on the addition of copper [12-15]. A previous study reported that the addition of $CuBr_2$ and NaCl to perovskite precursor solutions improved the conversion efficiency and durability of the devices [16-17]. In that study, it was reported that the lattice distortion of perovskite crystals was reduced by the addition of a small quantity of Cu, and the lattice defects were suppressed by the transfer of Na to the lattice defect sites after the desorption of methylammonium (MA), which led to the enhanced conversion efficiency and durability of the devices.

In addition to the experimental investigation of the addition effect, the analysis using first-principles calculations has been actively studied. $CH_3NH_3PbI_3$ is known as the most general perovskite used as a photoelectric conversion material. First-principles calculations using a structural model in which organic cations, metal cations, and halogen anions are substituted by other molecules or atoms can be used to estimate the stability of the crystal structure. In a previous study reported in 2019, first-principles calculations showed that substituting EA for MA enhanced the stability of the crystal structure [18].

The calculated energy gap values were agreed well with the experimental values, and the correspondence between the calculated and experimental results indicates that the addition effect can be estimated by first-principles calculations. There have been other attempts to improve the properties of devices by substituting MA with larger organic cations [19-24]. Furthermore, numerous studies on the effects of halogen additions have been conducted, both computationally and experimentally [25-29]. The selectivity of the halogen is very important because the energy gap and the crystallinity of the perovskite film changes for halogen.

The purpose of this study is to investigate the addition effects of Cu, Na and EA using experimental characterization and first-principles calculations. Co-addition of Cu and Na enhanced the J_{SC}, V_{OC}, and *FF*, resulting in higher conversion efficiency. This result is attributed to the enhancement of carrier generation by Cu addition and the suppression of carrier loss by Na addition. The properties are expected to be further improved by using other organic cations or alkali metals, or by optimizing the experimental conditions.

2. Experimental procedures and calculation

Detailed fabrication processes were described in the previous works [30-33]. F-doped tin oxide (FTO) substrates were cleaned in an ultrasonic bath with acetone and methanol and dried under nitrogen gas. The 0.15 M TiO_2 precursor solution was spin-coated on the FTO substrate at 3000 rpm for 30 s, and the coated substrate was then annealed at 125 °C for 5 min. The 0.30 M TiO_2 precursor solution was spin-coated on the TiO_2 layer at 3000 rpm for 30 s, and the resulting substrate was annealed at 125 °C for 5 min. The process to form the 0.30 M precursor layer was performed twice. Then, the FTO substrate was sintered at 550 °C for 30 min to form a compact TiO_2 layer. To form the mesoporous TiO_2 layer, a TiO_2 paste was prepared from the TiO_2 powder with poly(ethylene glycol)in ultrapure water. The solution was mixed with acetylacetone and Triton X-10 for 30 min. Then, the TiO_2 paste was spin-coated on the compact TiO_2 layer at 5000 rpm for 30 s. The resulting cell was annealed at 550 °C for 30 min to form the mesoporous TiO_2 layer.

To prepare the perovskite compounds, mixed solutions of CH_3NH_3I (2.4 M, Showa Chemical, Tokyo, Japan) and $PbCl_2$ (0.8 M, Sigma-Aldrich, St. Louis, MO, USA) in *N,N*-dimethylformamide (DMF, Sigma-Aldrich, 0.5 mL) were prepared for the standard cell. Pb or MA in the perovskite structure was expected to be substituted by Cu, Na or EA, respectively. These perovskite solutions were then introduced into the TiO_2 mesopores by spin-coating at 2000 rpm for 60 s, which is followed by annealing in air. During the spin-coating, a hot air-blowing method was applied. Temperatures of the cells during the air-blowing were set at 90 °C. A polysilane solution was prepared by mixing chlorobenzene (Fujifilm Wako Pure Chemical Corporation, 0.5 mL) with decaphenylcyclopentasilane (DPPS, Osaka Gas Chemicals, OGSOL SI-30-10, 10 mg). During the last 15 s of the third spin-coating of the perovskite precursor solutions, the DPPS solution was also spin-coated on the perovskite layer [34-37]. The annealing temperature was gradually increased from 90 °C until the entire film turned black [38].

A solution of spiro-OMeTAD in chlorobenzene was mixed with a solution of lithium bis(tri-fluoromethylsulfonyl)imide in acetonitrile and tris(2-(1H-pyrazol-1-yl)-4-*tert*-butyl pyridine)cobalt(III) tri[bis(trifluoromethane)sulfonimide] in acetonitrile (0.5 mL) for 24 h. The former solution with 4-tertbutylpyridine was mixed with the Li-TFSI solution and FK209 solution (0.004 mL) for 30 min at 70 °C. Then, the spiro-OMeTAD solution was spin-coated on the perovskite layer at 4000 rpm for 30 s. All procedures were performed in ambient air. Finally, gold (Au) electrodes were evaporated as top electrodes using a metal mask for the patterning.

First principle calculations of all structures were performed within the generalized gradient approximation in the form of the Perdew-Burke-Ernzerhof exchange-correlation functional using Quantum Espresso. The cut-off energy of the planar wavefunction was set to 80 eV for the structural optimization and to 25 eV for the other calculations. 4 × 4 × 4 *k*-point mesh was used for calculations of all structures.

3. Results and discussion

The band structure, partial density of states and parameters were obtained by first-principles calculations. The total substitution structure model used in the calculations is shown in Fig. 1. The energy gap increases when iodine is substituted with bromine or chlorine compared to MAPbI$_3$, which is the most general perovskite used as a photoelectric conversion material. In general, an increase in the energy gap may lead to an increase in the open-circuit voltage, therefore, the use of bromide or chloride as an additive may improve the open-circuit voltage.

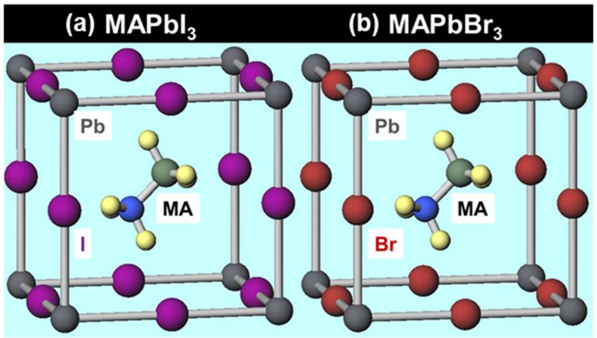

Figure 1. Structure models of (a) MAPbI$_3$, (b) MAPbBr$_3$.

The total energy per cell of the structural model is obtained by first-principles calculations, and a smaller value means that the crystal structure is more stable. Since the total energy decreases by substituting iodine with bromine or chlorine, the crystal structure is expected to be stabilized. The result that the addition of EA improves the stability of the crystal structure is in good agreement with previous studies.

Calculations for the partial substitutional structure model were also performed [39-41]. The partial substitution structure model used in the calculations is shown in Fig. 2. Compared to the total substitutional structure model, the partial substitutional structure model contains more atoms, and thus requires a longer time for calculation. In contrast to MA$_{0.875}$EA$_{0.125}$PbI$_3$, the addition of copper resulted in the formation of a shallow band of Cu d-orbitals slightly above the band of iodine p-orbitals, decreasing the energy gap and the mobility of holes. Furthermore, comparing MA$_{0.875}$EA$_{0.125}$Pb$_{0.875}$Cu$_{0.125}$I$_3$ and MA$_{0.750}$EA$_{0.125}$Na$_{0.125}$Pb$_{0.875}$Cu$_{0.125}$I$_3$, by substituting Na for a part of MA, a band of Na s orbitals is formed slightly above the conduction band minimum, which results in a slight increase in electron mobility. The energy gap is increased by substituting some of the iodine with bromine, and this result is in good agreement with the calculated results of the total substitution structure model.

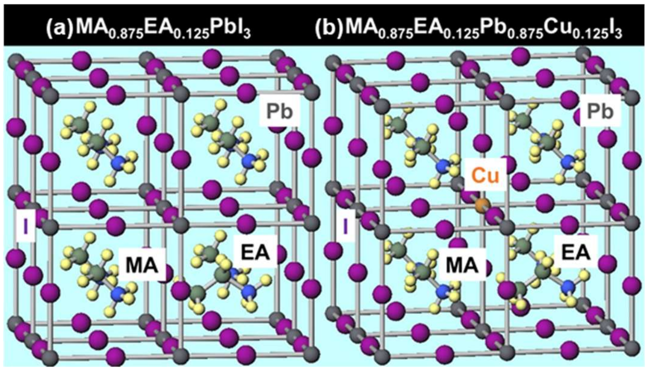

Figure 2. Partial substitution structure models of (a) MA$_{0.875}$EA$_{0.125}$PbI$_3$ and (b) MA$_{0.875}$EA$_{0.125}$Pb$_{0.875}$Cu$_{0.125}$I$_3$.

In the calculated results of the partial substitution structure model, it is indicated that the addition of Cu forms a shallow band of Cu d-orbitals slightly above the band of iodine p-orbitals, which reduces the energy gap and decreases the hole mobility. However, if we consider the Cu d-orbital band as an acceptor level, it may have a positive effect on the performance of the device.

The current-voltage (*J-V*) curve and the external quantum efficiency (EQE) obtained from the present perovskite photovoltaic devices. From the calculated results of the partial substitution structure model, it was expected that the addition of Cu would decrease the energy gap and reduce the hole mobility. However, from the measured results, the co-adding of Cu and Na slightly increased the energy gap and further enhanced the short-circuit current density, open-circuit voltage, and fill factor, resulting in higher conversion efficiency. Therefore, the Cu d-orbitals are considered to function as acceptor levels.

4. Conclusion

In this study, the effects of co-addition of Cu, Na and EA into the perovskite precursor solution were investigated using the first-principles calculations. The addition of these additives to the perovskite precursor solution increased the energy gap and improved the open circuit voltage in all devices compared to the standard system. According to first-principles calculations, replacing all of the iodine with bromine or chlorine increased the energy gap, indicating that the improvement in V_{OC} was due to the effect of halogen. When some of the lead was substituted with Cu, a shallow band of Cu d-orbitals was formed slightly above the valence band maximum, suggesting that the addition of Cu decreases the energy gap and reduces the hole mobility. When a small amount of Cu was added in the experiment, the conversion efficiency decreased slightly, but the energy gap increased slightly. This suggests that the Cu energy levels of formed in the forbidden band may function as acceptor levels. The excitation of electrons from the p-orbital of iodine to the d-orbital of Cu is thought to have promoted the generation of carriers, leading to the improvement of J_{SC}.

Author Contributions: Conceptualization, R.O. and T.O.; Methodology, R.O., T.O., and A.S.; Formal Analysis, R.O., T.O., and A.S.; Investigation, R.O. and A.S.; Resources, M.O., S.F., T.T., and T.H.; Data Curation, R.O. and T.O.; Writing—Original Draft Preparation, R.O. and T.O.; Writing—Review & Editing, R.O., T.O., A.S., M.O., S.F., T.T., and T.H.; Project Administration, T.O.; Funding Acquisition, T.O.

Funding: This research was partly funded by a Grant-in-Aid for Scientific Research (C) 21K04809.

Conflicts of Interest: The authors declare no conflicts of interest.

References

1. Bohr, C.; Le, K.; Fischer, T.; Mathur, S. Triaxial perovskite composite fibers spinning the way to flexible solar cells. *Adv. Eng. Mater.* 2021, 2100773, doi: 10.1002/adem.202100773.
2. Aliyaselvam, O. V.; Arith, F.; Mustafa, A. N.; Nor, M. K.; Al-Ani, O. A. Solution processed of solid state HTL of CuSCN layer at low annealing temperature for emerging solar cell. *IJRER* 2021, *11*, doi: 10.37934/arfmts.78.2.153159.
3. Islam, M. A.; Wahab, Y.A.; Khandaker, M. U.; Alsubaie, A.; Almalki, A. S. A.; Bradley, D. A.; Amin, N. High mobility reactive sputtered CuxO thin film for highly efficient and stable perovskite solar cells. *Crystals* 2021, *11*, 389, doi: org/10.3390/cryst11040389.
4. Salah, M. M.; Abouelatta, M.; Shaker, A.; Hassan, K. M.; Saeed, A. A comprehensive simulation study of hybrid halide perovskite solar cell with copper oxide as HTM. *Semicond. Sci. Technol.* 2019, *34*, 115009, doi: org/10.1088/1361-6641/ab22e1.
5. Haider, S. Z.; Anwar, H.; Wang, M. A comprehensive device modelling of perovskite solar cell with inorganic copper iodide as hole transport material. *Semicond. Sci. Technol.* 2018, *33*, 035001, doi: org/10.1088/1361-6641/aaa596.
6. Pitriana, P.; Wungu, T. D. K.; Herman; Hidayat, R. The characteristics of band structures and crystal binding in all-inorganic perovskite APbBr3 studied by the first principle calculations using the Density Functional Theory (DFT) method. *Results in Physics* 2019, *15*, 102592, doi: org/10.1016/j.rinp.2019.102592.

7. Chang, C.; Zou, X.; Cheng, J.; Ling, T.; Yao, Y.; Chen, D. Applied trace alkali metal elements for semiconductor property modulation of perovskite thin films. *Molecules* 2019, *24*, 4039, doi: 10.3390/molecules24224039.
8. Xiang, S.; Li, W.; Wei, Y.; Liu, J.; Liu, H.; Zhu, L.; Yang, S.; Chen, H. Natrium doping pushes the efficiency of carbon-based $CsPbI_3$ perovskite solar cells to 10.7%. *iScience* 2019, *15*, 156-164, doi: org/10.1016/j.isci.2019.04.025.
9. Qiao, L.; Fang, W. H.; Long, R.; Prezhdo, O. V. Alkali metals extend carrier lifetimes in lead halide perovskites by passivating and eliminating halide interstitial defects. *Angewandte Chemie* 2020, *132*, 4714-4720, doi: org/10.1002/ange.201911615.
10. Zhao, W.; Yao, Z.; Yu, F.; Yang, D.; Liu, S. Alkali metal doping for improved $CH_3NH_3PbI_3$ perovskite solar cells. *Adv. Sci.* 2018, *5*, 1700131, doi: 10.1002/advs.201700131.
11. Boopathi, K. M.; Mohan, R.; Huang, T. Y.; Budiawan, W.; Lin, M. Y.; Lee, C. H.; Ho, K. C.; Chu, C. W. Synergistic improvements in stability and performance of lead iodide perovskite solar cells incorporating salt additives. *Mater. Chem. A* 2016, *4*, 1591, doi: 10.1039/c5ta10288j.
12. Wang, K. L.; Wang, R.; Wang, Z. K.; Li, M.; Zhang, Y.; Ma, H.; Liao, L. S.; Yang, Y. Tailored phase transformation of $CsPbI_2Br$ films by copper (II) bromide for high-performance all-inorganic perovskite solar cells. *Nano Lett.* 2019, *19*, 5176-5184, doi: org/10.1021/acs.nanolett.9b01553.
13. Li, M.; Wang, Z. K.; Zhuo, M. P.; Hu, Y.; Hu, K. H.; Ye, Q. Q.; Jain, S. M.; Yang, Y. G.; Gao, X. Y.; Liao, L. S. Pb–Sn–Cu Ternary organometallic halide perovskite solar cells. *Adv. Mater.* 2018, 1800258, doi: 10.1002/adma.201800258.
14. Elseman, A. M.; Shalan, A. E.; Sajid, S.; Rashad, M. M.; Hassan, A. M.; Li, M. Copper-substituted lead perovskite materials constructed with different halides for working $(CH_3NH_3)_2CuX_4$-based perovskite solar cells from experimental and theoretical view. *ACS Appl. Mater. Interfaces* 2018, *10*, 11699-11707, doi: org/10.1021/acsami.8b00495.
15. Jahandar, M.; Heo, J. H.; Song, C. E.; Kong, K. J.; Shin, W. S.; Lee, J. C.; Im, S. H.; Moon, S. J. Highly efficient metal halide substituted $CH_3NH_3I(PbI_2)_{1-X}(CuBr_2)_X$ planar perovskite solar cells. *Nano Energy* 2016, *27*, 330-339, doi: org/10.1016/j.nanoen.2016.07.022.
16. Ueoka, N.; Oku, T. Effects of co-addition of sodium chloride and copper (II) bromide to mixed-cation mixed-halide perovskite photovoltaic devices. *ACS Appl. Energy Mater.* 2020, *3*, 7272-7283, doi: org/10.1021/acsaem.0c00182
17. Ueoka, N.; Oku, T.; Suzuki, A. Additive effects of alkali metals on Cu-modified $CH_3NH_3PbI_{3-\delta}Cl_\delta$ photovoltaic devices. *RSC Adv.* 2019, *9*, 24231, doi: 10.1039/c9ra03068a.
18. Liu, D.; Li, Q.; Wu, K. Ethylammonium as an alternative cation for efficient perovskite solar cells from first-principles calculations. *RSC Adv.* 2019, *9*, 7356, doi: 10.1039/c9ra00853e.
19. Jung, M. H. Formation of cubic perovskite alloy containing the ammonium cation of 2D perovskite for high performance solar cells with improved stability. *RSC Adv.* 2021, *11*, 32590, doi: 10.1039/d1ra04520b.
20. Bidikoudi, M.; Simal, C.; Dracopoulos, V.; Stathatos, E. Exploring the effect of ammonium iodide salts employed in multication perovskite solar cells with a carbon electrode. *Molecules* 2021, *26*, 5737, doi: org/10.3390/molecules26195737.
21. Mateen, M.; Arain, Z.; Liu, X.; Iqbal, A.; Ren, Y.; Zhang, X.; Liu, C.; Chen, Q.; Ma, S.; Ding, Y.; Cai, M.; Dai, S. Boosting optoelectronic performance of MAPbI3 perovskite solar cells via ethylammonium chloride additive engineering. *Sci. China Mater.* 2020, *63*, 2477-2486, doi: org/10.1007/s40843-020-1383-3.
22. Zhang, Y.; Kim, S. G.; Lee, D.; Shin, H.; Park, N. G. Bifacial stamping for high efficiency perovskite solar cells. *RSC Energy Environ. Sci.* 2019, *12*, doi: 10.1039/c8ee02730g.
23. Dhar, A.; Dey, A.; Maiti, P.; Paul, P. K.; Roy, S.; Paul, S.; Vekariya, R. L. Fabrication and characterization of next generation nano-structured organo-lead halide-based perovskite solar cell. *Ionics* 2018, *24*, 1-7, doi: 10.1007/s11581-017-2256-x.
24. Nishi, K.; Oku, T.; Kishimoto, T.; Ueoka, N.; Suzuki, A. Photovoltaic characteristics of $CH_3NH_3PbI_3$ perovskite solar cells added with ethylammonium bromide and formamidinium iodide. *Coatings* **2020**, 10 410−1−10, doi:10.3390/coatings10040410.
25. Li, Q.; Zhao, Y.; Zhou, W.; Han, Z.; Fu, R.; Lin, F.; Yu, D.; Zhao, Q. Halogen engineering for operationally stable perovskite solar cells via sequential deposition. *Adv. Energy Mater.* 2019, *9*, 1902239, doi: 10.1002/aenm.201902239.
26. Mohebpour, M. A.; Saffari, M.; Soleimani, H. R.; Tagani, M. B. High performance of mixed halide perovskite solar cells: role of halogen atom and plasmonic nanoparticles on the ideal current density of cell. *Physica E: Low-dimensional Systems and Nanostructures* 2018, *97*, 282-289, doi: org/10.1016/j.physe.2017.11.022.
27. Lee, A. Y.; Park, D. Y.; Jeong, M. S. Correlational study of halogen tuning effect in hybrid perovskite single crystals with Raman scattering, X-ray diffraction, and absorption spectroscopy. *Alloys and Compounds* 2018, *738*, 239-245, doi: org/10.1016/j.jallcom.2017.12.149.
28. Motta, C.; El-Mellouhi, F.; Sanvito, S. Charge carrier mobility in hybrid halide perovskites. *Scientific Reports* 2015, *5*, 12746, doi: 10.1038/srep12746.
29. Park, B. W.; Jain, S. M.; Zhang, X.; Hagfeldt, A.; Boschloo, G.; Edvinsson, T. Resonance raman and excitation energy dependent charge transfer mechanism in halide-substituted hybrid perovskite solar cells. *ACS Nano*, 2015, *9*, 2088-2101, doi: org/10.1021/nn507345e.
30. Oku, T.; Zushi, M.; Imanishi, Y.; Suzuki, A.; Suzuki, K. Microstructures and photovoltaic properties of perovskite-type $CH_3NH_3PbI_3$ compounds. *Appl. Phys. Express* **2014**, *7*, 121601, doi:10.7567/APEX.7.121601.
31. Oku, T.; Nomura, J.; Suzuki, A.; Tanaka, H.; Fukunishi, S.; Minami, S.; Tsukada, S. Fabrication and characterization of $CH_3NH_3PbI_3$ perovskite solar cells added with polysilanes. *Int. J. Photoenergy* **2018**, 8654963, doi:10.1155/2018/8654963.

32. Oku, T.; Ohishi, Y.; Ueoka, N. Highly (100)-oriented $CH_3NH_3PbI_3(Cl)$ perovskite solar cells prepared with NH_4Cl using an air blow method. *RSC Adv.* **2018**, *8*, 10389–10395, doi:10.1039/c7ra13582c.
33. Oku, T. Crystal structures of perovskite halide compounds used for solar cells. *Rev. Adv. Mater. Sci.* **2020**, *59*, 264–305, doi:10.1515/rams-2020-0015.
34. Taguchi, M.; Suzuki, A.; Oku, T.; Ueoka, N.; Minami, S.; Okita, M. Effects of annealing temperature on decaphenylcyclopentasilane-inserted $CH_3NH_3PbI_3$ perovskite solar cells. *Chem. Phys. Lett.* **2019**, *737*, 136822, doi:10.1016/j.cplett.2019.136822.
35. Oku, T.; Kandori, S.; Taguchi, M.; Suzuki, A.; Okita, M.; Minami, S.; Fukunishi, S.; Tachikawa, T. Polysilane-inserted methylammonium lead iodide perovskite solar cells doped with formamidinium and potassium. *Energies* **2020**, *13*, 4776, doi:10.3390/en13184776.
36. Suzuki A.; Taguchi M.; Oku T.; Okita M.; Minami S.; Fukunishi S.; Tachikawa T., Additive effects of methyl ammonium bromide or formamidinium bromide in methylammonium lead iodide perovskite solar cells using decaphenylcyclopentasilane, *J. Mater. Sci.: Mater. Electron.* **2021**, *32*, 26449–26464, doi:10.1007/s10854-021-07023-w.
37. Oku, T.; Taguchi, M.; Suzuki, A.; Kitagawa, K.; Asakawa, Y.; Yoshida, S.; Okita, M.; Minami, S.; Fukunishi, S.; and Tachikawa, T.; Effects of polysilane addition to chlorobenzene and high temperature annealing on $CH_3NH_3PbI_3$ perovskite photovoltaic devices. *Coatings* **2021**, *11*, 665, doi:10.3390/coatings11060665.
38. Huang, L.; Hu, Z.; Xu, J.; Zhang, K.; Zhang, J.; Zhu, Y. Multi-step slow annealing perovskite films for high performance planar perovskite solar cells. *Solar Energy Materials & Solar Cells* 2015, *141*, 377-382, doi: org/10.1016/j.solmat.2015.06.018.
39. Ueoka, N.; Oku, T.; Suzuki, A. Effects of doping with Na, K, Rb, and formamidinium cations on $(CH_3NH_3)_{0.99}Rb_{0.01}Pb_{0.99}Cu_{0.01}I_{3-x}(Cl, Br)_x$ perovskite photovoltaic cells. *AIP Adv.* **2020**, *10*, 125023, doi: 10.1063/5.0029162.
40. Suzuki A.; Kitagawa K.; Oku T.; Okita M.; Fukunishi S.; Tachikawa T., Additive effects of copper and alkali metal halides into methylammonium lead iodide perovskite solar cells, *Electron. Mater. Lett.* **2021**, doi: 10.1007/s13391-021-00325-5.
41. Suzuki A.; Oku T., Effects of mixed-valence states of Eu-doped $FAPbI_3$ perovskite crystals studied by first-principles calculation, *Mater. Adv.*, **2021**, 2, 2609-2616, doi:10.1039/D0MA00994F.